Spin-singlet ground state of the coupled $J_{\mathrm{eff}} = \frac{1}{2}$ alternating chain system Sr$_2$Co(SeO$_3$)$_3$

I. Panneer Muthuselvam [1,*] R. Madhumathy,[2] K. Saranya,[2] K. Moovendaran [3] Suheon Lee,[4] Kwang-Yong Choi [5]
Wei-tin Chen [6,7] Chin-Wei Wang [8] Peng-Jen Chen,[9,10] M. Ponmurugan,[2] Min-nan Ou [3]
Yang-Yuan Chen,[3] Heung-Sik Kim,[11] and R. Sankar[3,†]

[1]*Department of Physics (MMV), Banaras Hindu University, Varanasi-221005, Uttar Pradesh, India*
[2]*Department of Physics, School of Basic and Applied Sciences, Central University of Tamil Nadu,*
Neelakudi, Thiruvarur 610005, Tamil Nadu, India
[3]*Institute of Physics, Academia Sinica, Taipei 10617, Taiwan*
[4]*Center for Integrated Nanostructure Physics, Institute for Basic Science (IBS), Suwon 16419, Republic of Korea*
[5]*Department of Physics, Sungkyunkwan University, Suwon 16419, Republic of Korea*
[6]*Center for Condensed Matter Sciences, National Taiwan University, Taipei 10617, Taiwan*
[7]*Taiwan Consortium of Emergent Crystalline Materials, Ministry of Science and Technology, Taipei 10622, Taiwan*
[8]*National Synchrotron Radiation Research Center, Hsinchu 30076, Taiwan*
[9]*Department of Mechanical Engineering, City University of Hong Kong, Hong Kong, 999077, China*
[10]*Hong Kong Institute for Advanced Study, City University of Hong Kong, Hong Kong, 999077, China*
[11]*Department of Physics and Institute of Quantum Convergence Technology,*
Kangwon National University, Chuncheon 24311, Republic of Korea

We report a detailed study of the structural, magnetic, thermodynamic, and electronic properties of a coupled $J_{\mathrm{eff}} = \frac{1}{2}$ alternating chain Sr$_2$Co(SeO$_3$)$_3$ compound using magnetic susceptibility $\chi(T)$, magnetic specific heat $C_{\mathrm{m}}(T)$, magnetization, and neutron diffraction measurements along with first-principles calculations. The first-principles calculations based on the density functional theory suggest that Sr$_2$Co(SeO$_3$)$_3$ forms a quasi-one-dimensional chain with bond alternation and interchain interactions. $\chi(T)$, $C_{\mathrm{m}}(T)$, and neutron powder diffraction measurements confirm that no long-range magnetic ordering occurs down to 100 mK. Instead, a maximum in $\chi(T)$ and $C_{\mathrm{m}}(T)$ and an exponential drop of $\chi(T)$ and $C_p(T)$ as $T \to 0$ K point to a spin-singlet ground state. The analysis of $\chi(T)$ and $C_{\mathrm{m}}(T)$ based on a J_1-J_2 alternating Heisenberg model shows the bond alternation $\alpha = J_2/J_1 \approx 0.7$ and a spin gap of $\Delta \approx 3$ K. Our work demonstrates that Sr$_2$Co(SeO$_3$)$_3$ is a coupled alternating chain system based on spin-orbit entangled $J_{\mathrm{eff}} = \frac{1}{2}$.

I. INTRODUCTION

One-dimensional (1D) spin-$\frac{1}{2}$ chain systems have attracted longstanding interest as they can harbor diverse quantum many-body phenomena [1–4]. For instance, uniform 1D chains evade any symmetry breaking down to $T = 0$ K and feature a Tomonaga-Luttinger spin liquid where spin-spin correlation decays algebraically with distance [5]. Alternating Heisenberg chains (AHCs) are a natural generalization of the 1D uniform spin chain by alternating two nearest-neighboring J_1 and J_2 interactions ($\alpha = J_2/J_1$). For $0 \leqslant \alpha < 1$, spin dimerization breaks translational symmetry, thereby giving rise to a spin-singlet ground state with gapped triplon excitations, multimagnon continua, and bound states [4,6–11].

From a material perspective, Cu^{2+} ($3d^9$), V^{4+} ($3d^1$), and Co^{2+} ($3d^7$) ions are sought after as potential hosts for spin-$\frac{1}{2}$ chain compounds. The Co^{2+} ion differs from the Cu^{2+} and V^{4+} elements (with spin only magnetic moments) in its strong

spin-orbit coupling and a uniaxial crystal field. In a certain octahedral environment, the high-spin Co^{2+} ion ($L = 3$ and $S = \frac{3}{2}$) hosts a $J_{\mathrm{eff}} = \frac{1}{2}$ Kramers doublet ground state [12,13]. In this context, the $J_{\mathrm{eff}} = \frac{1}{2}$ Co^{2+} spin systems are of particular interest because they often possess pronounced quantum fluctuations and anisotropic interactions.

(Ba,Sr)Co$_2$V$_2$O$_8$ is a representative example of a quasi-1D Ising-like antiferromagnet where Co^{2+} cations form a screw chain [14]. At zero field, these compounds undergo an antiferromagnetic (AFM) order at low temperatures. On application of an external magnetic field along the chain axis, a field-induced quantum phase transition occurs via an order-to-disorder mechanism [15,16]. Singularly, (Ba,Sr)Co$_2$V$_2$O$_8$ shows a variety of exotic phenomena: a bound state formation and spinon confinement [17,18], topological excitations [19], Bethe strings [20], and emergent fermions in a transverse field [21]. Another paradigmatic Ising chain is CoNb$_2$O$_6$, in which the magnetic Co^{2+} ions are arranged in zigzag chains [22]. In the low-T commensurate ordered state, a rich spectrum of nine bound states is observed in weak transverse fields. Near the transition point, E$_8$ symmetry emerges that dictates the excitation spectrum of the system. Remarkably, a recent study of
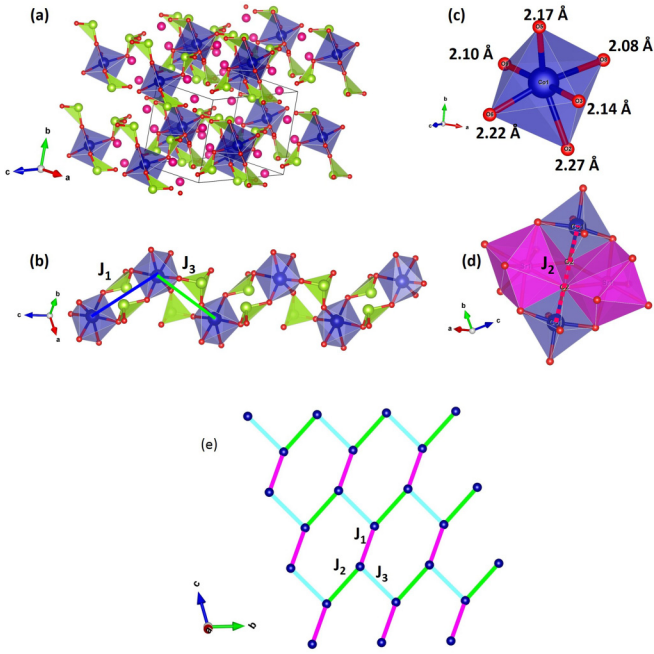
*ipmphysics@gmail.com
†sankarndf@gmail.com

FIG. 1. (a) Schematic crystal structure of $Sr_2Co(SeO_3)_3$ with the CoO_6 octahedra (blue) and the SeO_3 pyramidal (green). The magenta, blue, and red balls represent Sr, Co, and O ions, respectively. (b) Zig-zag chain along the c axis is formed through cornersharing of CoO_6 octahedra to SeO_3 pyramids. (c) CoO_6 octahedral coordination with Co-O distances. (d) Interlayer CoO_6 are connected through Sr-O polyhedra. (e) Schematic top view of the J_1-J_2 alternating chains coupled by weak interchain interaction J_3 in the bc plane. The drawn crystal structure is based on the neutron diffraction data collected at $T = 1.5$ K.

TABLE I. The atomic coordinates obtained from Rietveld refinement of room-temperature synchrotron powder XRD data of $Sr_2Co(SeO_3)_3$ crushed single crystals.

Atom	Site	X	Y	Z	Beq / A^2
Sr1	2i	0.2473(4)	0.0866(3)	0.3905(3)	0.59(7)
Sr2	2i	0.3691(4)	0.5141(3)	0.1921(3)	0.95(7)
Co1	2i	0.9074(5)	0.6599(5)	0.2464(4)	0.95(9)
Se1	2i	0.6361(4)	0.9175(3)	0.2053(3)	0.95(8)
Se2	2i	0.8977(4)	0.2097(3)	0.0410(3)	0.69(7)
Se3	2i	0.7660(4)	0.3631(4)	0.4170(3)	0.97(7)
O1	2i	0.4773(2)	0.8794(2)	0.2988(2)	1.2(1)
O2	2i	0.8592(2)	0.9522(2)	0.3406(2)	
O3	2i	0.6324(2)	0.7040(2)	0.0946(2)	
O4	2i	0.1242(2)	0.2513(2)	0.1644(2)	
O5	2i	0.8579(2)	0.4403(2)	0.1016(2)	
O6	12i	0.9380(2)	0.1708(2)	0.8607(2)	
O7	12i	0.5287(2)	0.2816(2)	0.3693(2)	
O8	12i	0.7487(2)	0.5819(2)	0.3888(2)	
O9	12i	0.8181(2)	0.3957(2)	0.6198(2)	

$CoNb_2O_6$ raises the possibility of dominant bond-dependent interactions, modeled as twisted Kitaev chains [23]. In this vein, a search for such exotic physics in Co^{2+}-based spin chains is highly desirable.

$Sr_2Co(SeO_3)_3$ is a candidate material of 1D $J_{eff} = \frac{1}{2}$ spin chain. $Sr_2Co(SeO_3)_3$ crystallizes in the triclinic structure [shown in Figs. 1(a)-1(d)] with $P\bar{1}$ space group and the lattice parameters $a=7.326$ Å, $b=7.605$ Å, $c=8.734$ Å, and $Z=2$ [24]. The crystal structure comprises three-dimensional networks of SrO_8 polyhedra, CoO_6 octahedra, and pyramidal SeO_3 groups. The CoO_6 octahedra are distorted with three longer Co-O distances of 2.1 Å to 2.6 Å and another three Co-O shorter distances of 2.04 - 2.09 Å. As shown in Fig. 1(b), the magnetic Co^{2+} ions in CoO_6 octahedra form zigzag-like chains by corner-sharing of their two edges through two nonmagnetic SeO_3 pyramids along the crystallographic c axis. Consequently, longer-range exchange paths between the Co^{2+} ions are expected to lead to weak magnetic interactions. Although the title compound has been synthesized in the last decade, magnetic characterizations are hitherto not reported [24].

In this paper, we present the structural, magnetic, and thermodynamics properties of $Sr_2Co(SeO_3)_3$ single crystal by combining magnetization, specific heat, and neutron diffraction measurements with first-principles calculations. We find that $Sr_2Co(SeO_3)_3$ forms coupled $J_{eff} = \frac{1}{2}$ AFM-AFM

alternating chain with $\alpha \approx 0.7$ and the spin gap is estimated to be $\Delta \approx 3$ K. Our work demonstrates that $Sr_2Co(SeO_3)_3$ constitutes a coupled AFM alternating chain system with spin-orbit entanglement.

II. EXPERIMENTAL DETAILS

Single crystals of $Sr_2Co(SeO_3)_3$ were grown using the hydrothermal method. The molar ratio 2:1:3 of $Sr(OH)_2$, $Co(OH)_2$ and SeO_2 were dissolved in distilled H_2O. The mixer solution was continuously stirred in the air, allowing for a homogenous solution. Then, the homogenous mixer was transferred into stainless steel Teflon autoclave. The closed autoclave was heated slowly up to 200 °C, maintained at 200 °C for 24 h, and then cooled at a rate of 1 °C/h up to 150 °C. Finally, the autoclave was cooled down to room temperature. The obtained products were collected and purified with distilled water and dried in the air at room temperature. A single crystal of $Sr_2Co(SeO_3)_3$ crystallizes with a violet color.

The quality of the crystal was analyzed by powder x-ray diffraction (XRD) technique at room temperature using a D8 diffractometer with Cu K$_\alpha$ radiation. In addition, a high-resolution synchrotron x-ray powder diffraction (SXRD) experiment was carried out for phase identification and structure analysis. The SXRD patterns were obtained with the MYTHEN detector with a 15 keV beam at beamline 09A, Taiwan Photon Source (TPS), National Synchrotron Radiation Research Center (NSRRC) in Taiwan. The powder sample was packed in a borosilicate capillary, and the capillary was kept spinning during data collection. A neutron powder diffraction (NPD) experiment was conducted at beamline ECHIDNA, Australian Nuclear Science and Technology Organisation (ANSTO), Australia. The sample was loaded in a vanadium can and the pattern was obtained at low temperatures with a wavelength of $\lambda = 2.4395$ Å (ECHIDNA). The collected patterns were analyzed with the Rietveld method using the program Bruker DIFFRAC.TOPAS. The elemental analysis was examined by electron probe microanalysis

TABLE II. The refinement results of the $T = 1.5$ K NPD patterns for $Sr_2Co(SeO_3)_3$. The lattice parameters are $a = 7.30770(5)$ Å, $b = 7.60235(5)$ Å, $c = 8.6995(5)$ Å, $\alpha = 103.176(4)°$, $\beta = 105.414(4)°$, and $\gamma = 95.555(6)°$, and $V = 447.24(5)$ Å^3.

Atom	Site	X	Y	Z	Beq / A^2
Sr1	2i	0.2390(3)	0.1038(3)	0.3937(2)	2.0(4)
Sr2	2i	0.3674(3)	0.5278(3)	0.1987(2)	
Co1	2i	0.9143(7)	0.6830(7)	0.2552(6)	1.1(1)
Se1	2i	0.6390(2)	0.9171(2)	0.2077(2)	0.5(3)
Se2	2i	0.9056(2)	0.2011(2)	0.0383(2)	
Se3	2i	0.7686(2)	0.3713(2)	0.4108(2)	
O1	2i	0.5032(3)	0.8878(4)	0.3308(3)	0.9(3)
O2	2i	0.8462(3)	0.9630(4)	0.3565(3)	
O3	2i	0.6450(3)	0.7081(3)	0.0951(3)	
O4	2i	0.0945(3)	0.2331(3)	0.1646(3)	
O5	2i	0.8358(3)	0.4201(3)	0.0719(2)	
O6	12i	0.9262(3)	0.1701(3)	0.8529(3)	
O7	12i	0.5144(3)	0.3105(3)	0.3464(3)	
O8	12i	0.7539(3)	0.5803(3)	0.4101(3)	
O9	12i	0.8130(3)	0.3428(4)	0.6040(3)	

(EPMA). EPMA analysis was taken at several spots on the crystal, which yields the following composition: Sr (14.03), Co (6.8), and Se (19.5). The EPMA result is consistent with the expected Sr:Co:Se stoichiometry of 2:1:3. It was found that no other elements were present in the compound except for Sr, Se, and Co. The magnetic measurements were conducted with a Quantum Design VSM-SQUID magnetometer. Field-dependent magnetization measurements were recorded at 2 K with a field sweep from 0 to 7 T. The specific heat measurements were carried out using a Quantum Design PPMS with a relaxation technique.

The first-principles calculations based on the density functional theory (DFT) were performed using Quantum Espresso [25] with experimental structural parameters obtained at room temperature. The cutoff energy of the plane wave expansion was 40 Ry, and a $6 \times 6 \times 6$ k mesh was used to sample the Brillouin zone. The DFT+U scheme [26] with $U = 3.0$ eV was adopted to account for the localized nature of the Co-d orbitals. The exchange interactions were estimated using the Heisenberg model $H = -\sum_{(i,j)} J_{ij} \mathbf{S}_i \cdot \mathbf{S}_j$. The extracted magnetic parameters are listed in Table III.

III. RESULTS AND DISCUSSION

A. Structural analysis

The room-temperature XRD pattern of $Sr_2Co(SeO_3)_3$ crystal oriented along the (001) plane is shown in Fig. 2. The inset
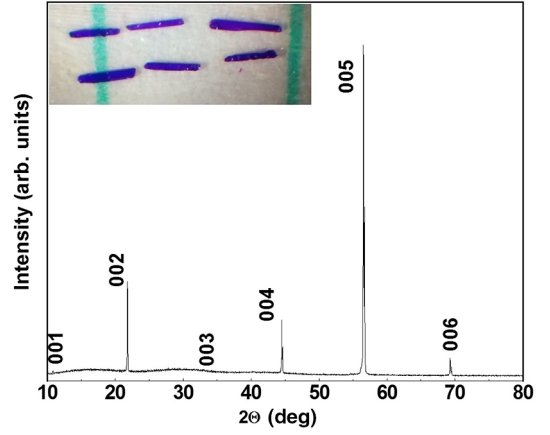

FIG. 2. X-ray diffraction pattern of $Sr_2Co(SeO_3)_3$ single crystal. The inset shows a photo of as-grown single crystals of $Sr_2Co(SeO_3)_3$.

illustrates the typical morphology image of $Sr_2Co(SeO_3)_3$ single crystals. The refined XRD pattern of powdered single crystals of $Sr_2Co(SeO_3)_3$ at room temperature showcases that all the diffraction peaks in the XRD pattern could be indexed with $P\bar{1}$ (No. 2) triclinic structure, as shown in Fig. 3(a), which is consistent with the previously reported structure [24]. The Rietveld refinement reveals that there is no trace of impurity obtained in the sample. The XRD results clearly show that the grown crystals have high quality. The refined lattice parameters at $T = 300$ K are $a = 7.33164(2)$ Å, $b = 7.61107(2)$ Å, $c = 8.73928(3)$ Å, $\alpha = 103.1851(2)°$, $\beta = 105.4875(2)°$, $\gamma = 95.5057(2)°$, and $V = 451.13(2)$ Å^3, in good agreement with those reported previously [24]. The refinement results of atomic coordination are tabulated in Table I. Further, the temperature-dependent NPD patterns were collected at a high-resolution neutron beamline ECHIDNA. Thermal shrinkage was shown at the low-temperature pattern, and the refinement result is exhibited in Fig. 3(b) and listed in Table II. Indeed, no magnetic peaks were observed at base temperature, indicating that no long-range magnetic ordering occurs down to $T = 1.5$ K.

B. Magnetic susceptibility and magnetization

Figure 4(a) presents the temperature dependencies of the field-cooled (FC) and zero-field-cooled (ZFC) magnetic susceptibilities $\chi(T)$ of $Sr_2Co(SeO_3)_3$ in a magnetic field of 1 T for $H \parallel c$ and $H \perp c$. $\chi(T)$ increases gradually with decreasing temperature and shows a maximum $T_m \sim 5.6$ K, indicating the onset of short-range magnetic or spin-singlet correlations. We detect no magnetic ordering down to 2 K. The FC and ZFC $\chi(T)$ curves perfectly overlap. Overall,

TABLE III. The exchange coupling parameters of $Sr_2Co(SeO_3)_3$, as shown in Fig. 1(b) and 1(d).

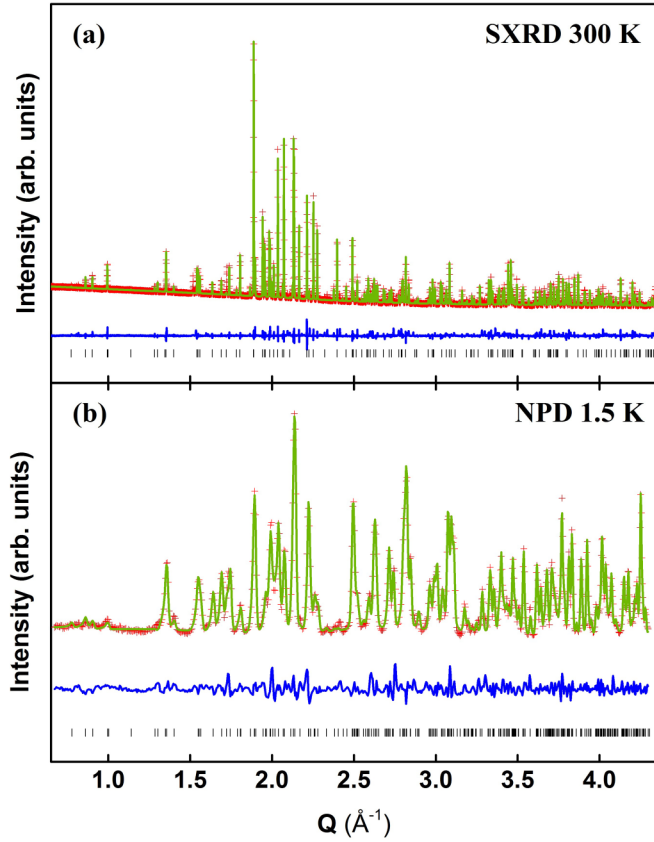| Exchange parameters	Distances Å				Co-Se/Sr-Co angle (deg)	Bond angle (deg)		Torsion angle (deg)
	Co-Co	Co-O	O···O	O-Co		Co-O···O	O···O-Co	Co-O···O-Co
$J_1 = -3.44$ K, AFM	5.198	2.155	2.634	2.087	93.80	149.4	105.1	36
$J_2 = -0.86$ K, AFM	5.440	2.276	2.795	2.276	98.17	92.91	92.91	180
$J_3 = -0.27$ K, AFM	5.541	2.227	2.735	2.106	115.62	134.42	124.32	36

FIG. 3. (a) Rietveld refinement fit with triclinic $P\bar{1}$ space group of crushed $Sr_2Co(SeO_3)_3$ single crystals using synchrotron powder x-ray diffraction at 300 K and (b) NPD pattern at 1.5 K. The observed, calculated, and difference patterns are shown in red crosses, and green and blue lines, respectively. The diffraction peaks are marked with black lines at the bottom of the figures.

we find a small difference between the $\chi_{\parallel c}(T)$ and $\chi_{\perp c}(T)$ data, indicating that magnetic anisotropy is not substantial. Thus, at first approximation, the magnetism of $Sr_2Co(SeO_3)_3$ is described within a Heisenberg model.

$\chi(T)$ is found to obey the Curie-Weiss (CW) law $\chi(T) = C/(T - \Theta_{CW})$ in two distinct temperature regimes, where C and Θ_{CW} are the Curie constant and CW temperature, respectively. In the high-T regime between 170 K and 400 K, we obtain the effective magnetic moment $\mu_{eff} = 4.77 \mu_B$ for $H \parallel c$ and 4.97 μ_B for $H \perp c$ from the CW fits to the inverse $1/\chi$ as shown in the dotted lines of Fig. 4(b). These values are much larger than the spin-only value of 1.73 μ_B expected for the $J_{eff} = \frac{1}{2}$ Co^{2+} ion. The observed large value of μ_{eff} points to the existence of unquenched orbital contribution of the Co^{2+} ion. Noteworthy is that the similar high value of μ_{eff} has been reported in the Co^{2+}-based spin-$\frac{1}{2}$ systems including $Ba_3CoTa_2O_9$ [27], $Na_2BaCo(PO_4)_2$ [28], and $BaCo_2(AsO_4)_2$ [29]. The switching CW behavior through 150 K alludes to the presence of local lattice distortions, which modify longer-range magnetic exchange paths [30]. In this situation, the low-T CW parameters are more appropriate to the magnetism of $Sr_2Co(SeO_3)_3$ than the high-T ones.

In order to understand the low-temperature magnetic behavior, the $1/\chi$ data in the temperature range between 45 K

and 140 K are fitted by the CW law. The fitting yields $\mu_{eff}^{\parallel c} = 5.1 \mu_B$, $\Theta_{CW}^{\parallel c} = -22$ K and $\mu_{eff}^{\perp c} = 5.6 \mu_B$, $\Theta_{CW}^{\perp c} = -17$ K. The negative value of Θ_{CW} indicates AFM exchange interactions between the $J_{eff} = \frac{1}{2}$ pseudospins.

Given that our first-principles calculations uncover bond alternation in $Sr_2Co(SeO_3)_3$ (see Sec. III D), we first attempt to analyze the observed $\chi(T)$ in terms of the theory developed for $S = 1/2$ alternating Heisenberg chains [31]:

$$\chi_{AHC}(T) = \frac{Ng^2\mu_B^2}{k_B T} \frac{A + Bx + Cx^2}{1 + Dx + Ex^2 + Fx^3}, \quad (1)$$

where $x = J_1/k_B T$ and the parameters $A, B, \cdots, F$ are polynomials of α (refer to Ref. [31] for the detailed functional form). The reasonable fit is obtained with the g factor of $g = 4.74(1)$, $J = -4.57$ K, and $\alpha = 0.68$ for $H \parallel c$ and $g = 5.49(1)$, $J = -4.8$ K, and $\alpha = 0.70$ for $H \perp c$ [see the blue and pink lines in Figs. 4(c) and 4(d)]. A close comparison between the experimental and calculated curves reveals a small discrepancy. As inferred from the weakly anisotropic $\chi(T)$ in Fig. 4(a), we invoke anisotropic exchange and interchain interactions as possible origins.

Figures 4(e) and 4(f) present the field and temperature dependence of $\chi(T, \mu_0 H)$ for $H \perp c$ and $H \parallel c$. With increasing field, the low-temperature $\chi(T, \mu_0 H)$ increases up to 4 T and T_m shifts towards lower temperatures. For fields above 4 T, $\chi(T, \mu_0 H)$ is gradually suppressed. This behavior indicates that $Sr_2Co(SeO_3)_3$ enters a fully polarized state at about $\mu_0 H_s = 4$ T.

Figure 5(a) exhibits the magnetization $M(H)$ curve measured from -7 T to 7 T at $T = 2$ K for $H \perp c$ and $H \parallel c$. With increasing field, the $M(H)$ curves initially show a linear increase in small fields and then a steep increase in the high-field region. Basically, the observed $M(H)$ curve is characteristic of a gapless spin chain. For an AHC, the energy gap is given by $\Delta = (1 - \frac{1}{2}\alpha - \frac{3}{8}\alpha^2 + \frac{1}{32}\alpha^3)J_1$ [9]. With the evaluated $\alpha = 0.64 - 0.70$ and $J_1 = -4.57 \sim -4.8$ K, we estimate $\Delta = (2.17 - 2.29)$ K. This value is comparable to the critical fields: $\mu_0 H_C^{\parallel c} = 3.07$ T and $\mu_0 H_C^{\perp c} = 2.73$ T from dM/dH in Fig. 5(b). Considering the measured temperature of $T = 2$ K, thermal populations may smear out the gap feature. We further determine the saturation fields $\mu_0 H_s^{\parallel c} \approx 4.4$ T and $\mu_0 H_C^{\perp c} \approx 4.7$ T. Above the saturation fields, $M(H)$ increases continuously due to the van Vleck paramagnetism.

C. Specific heat

The specific heat $C_p(T)$ of $Sr_2Co(SeO_3)_3$ single crystal is shown in Fig. 6(a). As evident from the log-log plot of $C_p(T)$ in Fig. 6(b), we observe no sharp peak down to 100 mK, excluding a phase transition to long-range magnetic ordering. Rather, the zero-field $C_p(T)$ features a broad hump at $T_m = 3$ K, reminiscent of a Schottky-like peak. With increasing field to 9 T (well above the saturation field), the low-temperature $C_p(T)$ is suppressed, while the maximum position shifts to a higher temperature. This trend supports the presence of a spin gap in the spectrum of magnetic excitations.

To extract the magnetic specific heat $C_m(T)$, the lattice contribution C_{ph} is subtracted from the total specific heat $C_m = C_p - C_{ph}$. We estimate the lattice contribution by
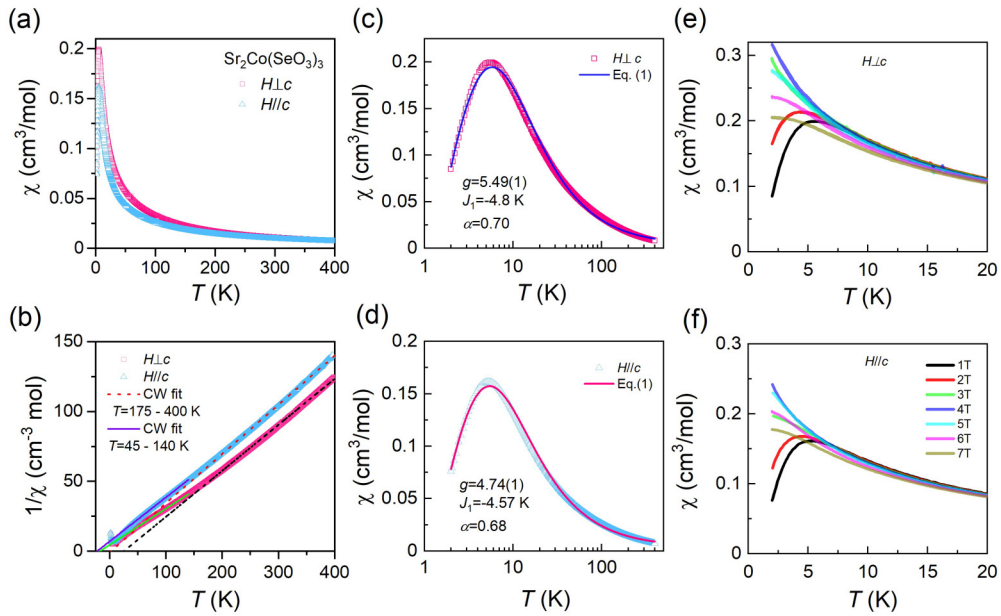
FIG. 4. (a) Temperature dependence of the static magnetic susceptibility $\chi(T)$ measured in a magnetic field $\mu_0 H = 1$ T for $H \perp c$ (pink squares) and $H \parallel c$ (cyan triangle) directions. (b) Temperature dependence of $1/\chi$ for $H \perp c$ and $H \parallel c$. The dotted and solid lines are Curie-Weiss fits to the high- and low-temperature $1/\chi(T)$. (c), (d) Fittings of $\chi(T)$ to an alternating spin model for $H \perp c$ and $H \parallel c$ as described in the main text. (e), (f) $\chi(T)$ measured under selected magnetic fields for $H \perp c$ and $H \parallel c$.

fitting the high-T $C_p(T)$ to a linear combination of the Debye (C_V^{Debye}) model and Einstein (C_V^{Einstein}) model [32] as $C_{\text{ph}} = k C_V^{\text{Debye}} + (1-k) C_V^{\text{Einstein}}$ with

$$C_V^{\text{Debye}} = 9nR\left(\frac{T}{\Theta_D}\right)^3 \int_0^{\Theta_D/T} \frac{x^4 e^x}{(e^x-1)^2} dx.$$

$$C_V^{\text{Einstein}} = 3nR\left(\frac{\Theta_E}{T}\right)^2 \frac{e^{\frac{\Theta_E}{T}}}{(e^{\frac{\Theta_E}{T}}-1)^2}.$$

Here, $x = \frac{\hbar\omega}{k_B T}$, Θ_D is the Debye temperature, Θ_E is the Einstein temperature, R is the molar gas constant, $n = 15$ is the total number of atoms in the formula unit of $Sr_2Co(SeO_3)_3$, and k represents the relative weight percentage of the Debye term to the Einstein term. The above expression describes the experimental data very well down to 2 K from 230 K [the red
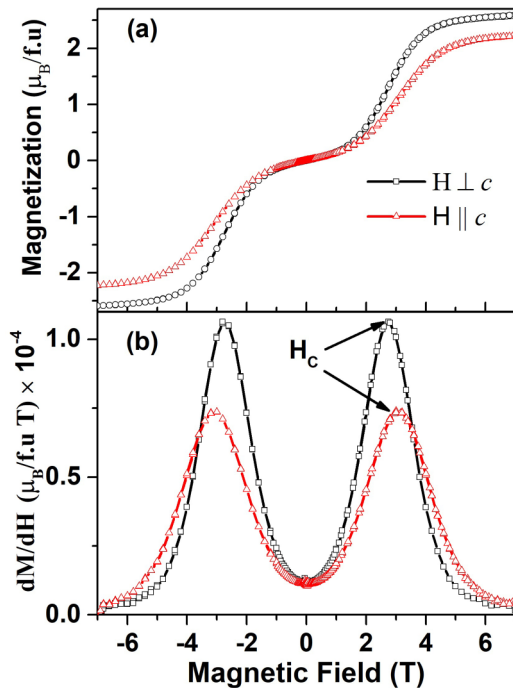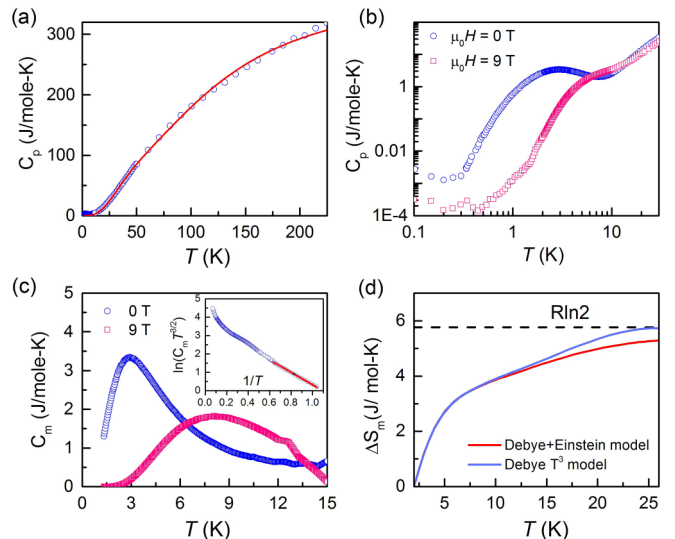

FIG. 5. (a) M-H curve of $Sr_2Co(SeO_3)_3$ at 2 K for $H \perp c$ and $H \parallel c$. (b) Derivative of magnetization curve, dM/dH versus H.

FIG. 6. (a) Temperature dependence of specific heat capacity $C_p(T)$ measured at zero field for $Sr_2Co(SeO_3)_3$. The solid line presents the phonon contribution described in the main text. (b) Log-log plot of the low-temperature $C_p(T)$ at $\mu_0 H = 0$ and 9 T. (c) Low-temperature magnetic specific heat $C_m(T)$ at $\mu_0 H = 0$ and 9 T. The inset is the plot of $\ln(C_m T^{3/2})$ versus $1/T$. The solid line is the best fit with the spin gap $\Delta/k_B = 3.3(7)$ K. (d) Magnetic entropy release ΔS_m as a function of temperature in zero magnetic field.

line in Fig. 6(a)] and is further extrapolated down to a hundred millikelvin temperature. The fitting parameters are given as $\Theta_D = 191 \pm 4$ K, $\Theta_E = 460 \pm 6$ K, and $k = 0.42 \pm 0.01$ which amounts to 42% of the Debye contribution to C_{ph}.

The low-temperature $C_m(T)$ is exhibited in Fig. 6(c). Both a Schottky-like anomaly and an exponential drop as $T \to 0$ K are clearly visible. With increasing field to 9 T, the maximum temperature of $C_m(T)$ increases to $T_m = 8.2$ K, forming a field-induced spin gap in the polarized phase. We now estimate the spin gap Δ using the relation [7]

$$C_m(T) \propto T^{-3/2} \exp(-\Delta/k_B T). \tag{2}$$

From fitting of the experimental $C_m(T)$ data to Eq. (2), as plotted in the inset of Fig. 6(c), we obtain $\Delta/k_B = 3.3 \pm 0.7$ K. This value lies in the range of the spin gap evaluated from the above $\chi(T)$ analysis and is consistent with the critical fields of 2.73–3.07 T determined by dM/dH.

Next, we derive the magnetic entropy S_m by integrating C_m/T over temperature. As shown in Fig. 6(d), the S_m is saturated at 26 K to the value of 5.32 J/(mol K), which is consistent with the theoretical value of $S_m = R \ln(2S + 1) = 5.76$ J/(mol K) for $S = 1/2$. Alternatively, we approximate the phonon contribution by the relation $C_p(T) = \gamma T + \beta T^3$ where γ is the Sommerfeld electronic coefficient and β is the phononic contribution. Since $Sr_2Co(SeO_3)_3$ is a magnetic insulator, $\gamma \approx 0$. Then, we obtain $\beta = 1.58$ mJ/mol K^4 from the fitting in the temperature range of $T = 10.25 - 19.25$ K. The above procedure yields the saturation to 5.72 J/(mol K) as plotted in the dashed line in Fig. 6(d). Noticeably, only 22% of the magnetic entropy is released at T_m. The rest of $S_m(T)$ is recovered gradually at high temperatures up to 28 K. Approximately 78% release of $S_m(T)$ above T_m implies that short-range order correlations or quantum fluctuations persist up to 28 K. Such a considerable fraction of the magnetic entropy gained above T_m is typical for quasi-1D magnetic systems. According to the theoretical prediction [10,33], the maximum value of $C_m/R = 0.38$ conveys information about the dimensionality of a system, being in excellent agreement with 0.35 for a quasi 1D system.

D. First-principles calculations of exchange interactions

Taking into account intrachain and interchain interactions, we estimated three important (J_1, J_2, J_3) possible magnetic exchange interactions through first-principles calculations. The calculated exchange couplings are summarized in Table III. The spin configuration of the ground state represents the antiparallel alignment of spins between two adjacent unit cells along the b direction, which results from the negative J_3. This result supports a coupled AFM-AFM alternating chain model with interchain interactions.

The coupling J_1 and J_2 involve only super-super exchange interaction Co-O$\cdots$O-Co, in which the magnetic exchange interaction (weak AFM, strong AFM, or FM) depends on the bridging angle between magnetic ions Co-O$\cdots$O and the distance between O$\cdots$O [34]. Without J_3, the magnetic structure would not be long-ranged in the present system.

Therefore, we consider the J_3 along the b axis. In J_3, no suitable connection Co-O$\cdots$O-Co can be formed, resulting in AFM interaction being small. Here, the strongest coupling does correspond to the shortest distance of O$\cdots$O and Co-Co in J_1. Remarkably J_2 coupling value is approximately several times higher than J_3. When looking at super-super exchange parameters in Table III, they are slightly varied in Co-O$\cdots$O angles and torsion angles. Therefore, this observation indicates that geometrical parameters alone cannot predict the strength of exchange coupling. We note that the calculated values J_i are somewhat smaller than the experimental values. In addition, the theoretically determined bond alternation $\alpha^{theo} \approx 0.25$ is larger than the experimental $\alpha^{exp} \approx 0.7$. One possible reason for this discrepancy is that the local atomic coordination varies with temperature, as inferred from the switching CW behavior in Fig. 4(b). On the other hand, the interchain interactions renormalize a spin gap, thereby increasing the bond alteration effectively. Since the alternating chains are coupled, α^{exp} should be regarded as an effective bond alternation.

IV. CONCLUSION

To conclude, we grew high-quality single crystals of $Sr_2Co(SeO_3)_3$ by hydrothermal method and characterized its magnetic properties. The $\chi(T)$, $C_p(T)$, and NPD experimental results reveal no magnetic phase transition down to 100 mK. Instead, a ground state is best described by a spin singlet with the energy of $\Delta \approx 3$ K within a coupled AFM-AFM alternating chain model. As such, $Sr_2Co(SeO_3)_3$ can serve as an alternating chain model system based on $J_{eff} = 1/2$. Given that the Luttinger liquid describes a field-induced gapless state, rich physics pertaining to quantum criticality can be explored. Our experimental results will motivate future experimental and theoretical studies to understand the possible effects of spin-orbit entanglement on magnetic excitations and spin dynamics.

[1] F. D. M. Haldane, Spontaneous dimerization in the S = $\frac{1}{2}$ Heisenberg antiferromagnetic chain with competing interactions, Phys. Rev. B **25**, 4925 (1982); Erratum: Spontaneous dimerization in the S = $\frac{1}{2}$ Heisenberg antiferromagnetic chain with competing interactions, **26**, 5257(E) (1982).

[2] G. Castilla, S. Chakravarty, and V. J. Emery, Quantum Magnetism of CuGeO$_3$, Phys. Rev. Lett. **75**, 1823 (1995).

[3] T. Masuda, A. Zheludev, B. Roessli, A. Bush, M. Markina, and A. Vasiliev, Spin waves and magnetic interactions in LiCu$_2$O$_2$, Phys. Rev. B **72**, 014405 (2005).

[4] C. S. Lue and B. X. Xie, NMR investigation of BaCu$_2$V$_2$O$_8$ in alternating-chain and dimer-chain model, Phys. Rev. B **72**, 052409 (2005).

[5] T. Giamarchi, *Quantum Physics in One Dimension* (Oxford University Press, Oxford, 2004).

[6] K. M. Diederix, H. W. J. Blöte, J. P. Groen, T. O. Klaassen, and N. J. Poulis, Theoretical and experimental study of the magnetic properties of the singlet-ground-state system Cu(NO$_3$)$_2$.2.5H$_2$O: An alternating linear Heisenberg antiferromagnet, Phys. Rev. B **19**, 420 (1979).

[7] J. C. Bonner, S. A. Friedberg, H. Kobayashi, D. L. Meier, and H. W. J. Blöte, Alternating linear-chain antiferromagnetism in copper nitrate Cu(NO$_3$)$_2$.2.5H$_2$O, Phys. Rev. B **27**, 248 (1983).

[8] M. Yamanaka, Y. Hatsugai, and M. Kohmoto, Phase diagram of the S= $\frac{1}{2}$ quantum spin chain with bond alternation, Phys. Rev. B **48**, 9555 (1993).

[9] T. Barnes, J. Riera, and D. A. Tennant, S= $\frac{1}{2}$ alternating chain using multiprecision methods, Phys. Rev. B **59**, 11384 (1999).

[10] D. C. Johnston, R. K. Kremer, M. Troyer, X. Wang, A. Klümper, S. L. Budko, A. F. Panchula, and P. C. Canfield, Thermodynamics of spin S= $\frac{1}{2}$ antiferromagnetic uniform and alternating-exchange Heisenberg chains, Phys. Rev. B **61**, 9558 (2000).

[11] S. S. Salunke, A. V. Mahajan, and I. Dasgupta, Magnetic properties and electronic structure of S = $\frac{1}{2}$ spin gap compound BaCu$_2$V$_2$O$_8$, Phys. Rev. B **77**, 012410 (2008).

[12] W. Low, Paramagnetic and optical spectra of divalent cobalt in cubic crystalline fields, Phys. Rev. **109**, 256 (1958).

[13] F. Lloret, M. Julve, J. Cano, R. Ruiz-García, and E. Pardo, Magnetic properties of six-coordinated high-spin cobalt (II) complexes: Theoretical background and its application, Inorg. Chim. Acta. **361**, 3432 (2008).

[14] S. Kimura, H. Yashiro, K. Okunishi, M. Hagiwara, Z. He, K. Kindo, T. Taniyama, and M. Itoh, Field-Induced Order-Disorder Transition in Antiferromagnetic BaCo$_2$V$_2$O$_8$ Driven by a Softening of Spinon Excitation, Phys. Rev. Lett. **99**, 087602 (2007).

[15] Z. He, T. Taniyama, T. Kyômen, and M. Itoh, Field-induced order-disorder transition in the quasi-one-dimensional anisotropic antiferromagnet BaCo$_2$V$_2$O$_8$, Phys. Rev. B **72**, 172403 (2005).

[16] Z. He, T. Taniyama and M. Itoh, Antiferromagnetic-paramagnetic transitions in longitudinal and transverse magnetic fields in a SrCo$_2$V$_2$O$_8$ crystal, Phys. Rev. B **73**, 212406 (2006).

[17] Z. Wang, M. Schmidt, A. K. Bera, A. T. M. N. Islam, B. Lake, A. Loidl, and J. Deisenhofer, Spinon confinement in the one-dimensional Ising-like antiferromagnet SrCo$_2$V$_2$O$_8$, Phys. Rev. B **91**, 140404(R) (2015).

[18] A. K. Bera, B. Lake, F. H. L. Essler, L. Vanderstraeten, C. Hubig, U. Schollwöck, A. T. M. N. Islam, A. Schneidewind,

and D. L. Quintero-Castro, Spinon confinement in a quasi-one-dimensional anisotropic Heisenberg magnet, Phys. Rev. B **96**, 054423 (2017).

[19] Q. Faure, S. Takayoshi, S. Petit, V. Simonet, S. Raymond, L. Regnault, M. Boehm, J. S. White, M. Månsson, C. Rüegg, P. Lejay, B. Canals, T. Lorenz, S. C. Furuya, T. Giamarchi, and B. Grenier, Topological quantum phase transition in the Ising-like antiferromagnetic spin chain BaCo$_2$V$_2$O$_8$, Nat. Phys. **14**, 716 (2018).

[20] Z. Wang, J. Wu, W. Yang, A. K. Bera, D. Kamenskyi, A. T. M. N. Islam, S. Xu, J. M. Law, B. Lake, C. Wu, and A. Loidl, Experimental observation of Bethe strings, Nature (London) **554**, 219 (2018).

[21] Z. Wang, J. Wu, S. Xu, W. Yang, C. Wu, A. K. Bera, A. T. M. Nazmul Islam, B. Lake, D. Kamenskyi, P. Gogoi, H. Engelkamp, N. Wang, J. Deisenhofer, and A. Loidl, From confined spinons to emergent fermions: Observation of elementary magnetic excitations in a transverse-field Ising chain, Phys. Rev. B **94**, 125130 (2016).

[22] T. Liang, S. M. Koohpayeh, J. W. Krizan, T. M. McQueen, R. J. Cava, and N. P. Ong, Heat capacity peak at the quantum critical point of the transverse Ising magnet CoNb$_2$O$_6$, Nat. Commun. **6**, 7611 (2015).

[23] C. M. Morris, N. Desai, J. Viirok, D. Hüvonen, U. Nagel, T. Rõõm, J. W. Krizan, R. J. Cava, T. M. McQueen, S. M. Koohpayeh, R. K. Kaul, and N. P. Armitage, Duality and domain wall dynamics in a twisted Kitaev chain, Nat. Phys. **17**, 832 (2021).

[24] M. Wildner, Preparation and crystal structure investigation of Sr$_2$Co(SeO$_3$)$_3$, J. Alloys Compd. **217**, 209 (1995).

[25] P. Giannozze *et al.*, QUANTUM ESPRESSO: A modular and open-source software project for quantum simulations of materials, J. Phys.: Condens. Matter **21**, 395502 (2009).

[26] V. I. Anisimov, F. Aryasetiawan, and A. I. Lichtenstein, First-principles calculations of the electronic structure and spectra of strongly correlated systems: The LDA+ U method, J. Phys.: Condens. Matter **9**, 767 (1997).

[27] K. M. Ranjith, K. Brinda, U. Arjun, N. G. Hegde, and R. Nath, Double phase transition in the triangular antiferromagnet Ba$_3$CoTa$_2$O$_9$, J. Phys.: Condens. Matter **29**, 115804 (2017).

[28] R. D. Zhong, S. Guo, G. Xu, Z. Xu, and R. J. Cava, Strong quantum fluctuations in a quantum spin liquid candidate with a Co-based triangular lattice, Proc. Natl. Acad. Sci. USA **116**, 14505 (2019).

[29] R. Zhong, T. Gao, N. P. Ong, and R. J. Cava, Weak-field induced nonmagnetic state in a Co-based honeycomb, Sci. Adv. **6**, eaay6953 (2020).

[30] J. Wang, W. Yuan, P. M. Singer, R. W. Smaha, W. He, J. Wen, Y. S. Lee, and T. Imai, Freezing of the Lattice in the Kagome Lattice Heisenberg Antiferromagnet Zn-Barlowite ZnCu$_3$(OD)$_6$FBr, Phys. Rev. Lett. **128**, 157202 (2022).

[31] J. W. Hall, W. E. Marsh, R. R. Weller, and W. E. Hatfield, Exchange coupling in the alternating-chain compounds catena-di-micron-chlorobis(4-methylpyridine)copper(II), catena-di-micron-bromobis-(N-methylimidazole)copper(II), catena-hexa nedionebis(thiosemicarbazato)copper(II), and catena-octaned ionebis(thiosemicarbazato)copper(II), Inorg. Chem. **20**, 1033 (1981).

[32] M. N. Ali, Q. D. Gibson, T. Klimczuk, and R. J. Cava, Non-centrosymmetric superconductor with a bulk three-dimensional

Dirac cone gapped by strong spin-orbit coupling, Phys. Rev. B **89**, 020505(R) (2014).

[33] B. Bernu and G. Misguich, Specific heat and high-temperature series of lattice models: Interpolation scheme and examples on quantum spin systems in one and two dimensions, Phys. Rev. B **63**, 134409 (2001).

[34] H.-J. Koo, D. Dai, and M.-H. Whangbo, Importance of supersuperexchange interactions in determining the dimensionality of magnetic properties. determination of strongly interacting spin exchange paths in $A_2Cu(PO_4)_2$ (A = Ba, Sr), $ACuP_2O_7$ (Ba, Ca, Sr, Pb), $CaCuGe_2O_6$, and $Cu_2UO_2(PO_4)_2$ on the basis of qualitative spin dimer analysis, Inorg. Chem. **44**, 4359 (2005).